Communication

Site-Selective Patterning Using Surfactant-Based Resists

Noshir S. Pesika, Fengqiu Fan, Peter C. Searson, and Kathleen J. Stebe

J. Am. Chem. Soc., **2005**, 127 (34), 11960-11962• DOI: 10.1021/ja050955n • Publication Date (Web): 09 August 2005

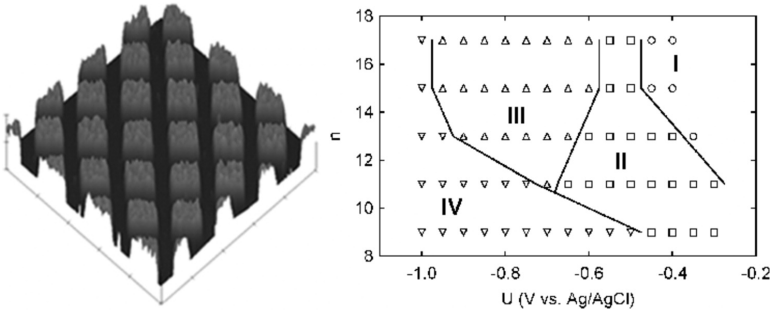

More About This Article

Additional resources and features associated with this article are available within the HTML version:

- Supporting Information
- Links to the 5 articles that cite this article, as of the time of this article download
- Access to high resolution figures
- Links to articles and content related to this article
- Copyright permission to reproduce figures and/or text from this article

View the Full Text HTML

J|A|C|S
COMMUNICATIONS

Published on Web 08/09/2005

Site-Selective Patterning Using Surfactant-Based Resists

Noshir S. Pesika,[†] Fengqiu Fan,[†] Peter C. Searson,*[,‡] and Kathleen J. Stebe*[,†]

Department of Chemical and Biomolecular Engineering and Department of Materials Science and Engineering, Johns Hopkins University, Baltimore, Maryland 21218

Received February 14, 2005; Revised Manuscript Received July 20, 2005; E-mail: searson@jhu.edu; kjs@jhu.edu

Patterned self-assembled monolayers (SAMs) formed by soft lithography allow surface properties to be tailored at the molecular level with lateral dimensions less than 100 nm. In microfluidics, patterned SAMs with hydrophilic and hydrophobic regions are used to direct fluid flow to the hydrophilic regions.[1,2] In biology, patterned SAMs with adhesive and nonadhesive regions are used to direct cell binding.[3,4] In materials science, patterned SAMs are used as etch resists to create trenches, wells, and posts in substrates.[5−7]

There have been very few reports where patterned SAMs formed by soft lithography[8] or electron beam irradiation[9−11] have been explored as resists for electrodeposition. Since these reports did not address the influence of deposition potential, chain length, or other experimental conditions, the potential for soft lithography and electrodeposition to create patterned structures is not well understood.

In this work, patterned SAMs of alkanethiols on gold or silver are explored as resists for electrodeposition, with surprisingly rich behavior depending on the overpotential and the length of the alkane chain. At small overpotentials, SAMs are positive resists with deposition only in the surfactant-free regions. At larger overpotentials, SAMs are negative resists with preferential deposition beneath the SAMs. Tunable surfactant-based resists are potentially versatile tools to dictate the deposition of materials and are demonstrated as a means of creating complex, three-dimensional structures.

In our experiments, patterned alkanethiol monolayers, (CH_3-$(CH_2)_n$SH with $n = 9-17$), were created on evaporated silver or gold films by soft lithography. Figure 1 shows features created by depositing silver in positive resist mode at −0.45 V (Ag/AgCl) on a patterned silver surface with 6 μm SAM-free squares at 10 μm center-to-center spacings. The friction force image (inset) taken before electrodeposition confirms that the surfactant, octadecanethiol (ODT), is present in a grid pattern with an array of 6 μm SAM-free squares. After deposition for about 90 min (0.28 C cm^{-2}), the optical microscope image shows an array of silver islands in the SAM-free squares, which preserve the lateral dimensions of the features. The AFM image (inset) shows that the islands are uniform with an average height of 800 nm, in excellent agreement with the value of 830 nm obtained from the deposition charge assuming no lateral growth and a deposition efficiency of 1.0. There is no evidence of lateral growth, even though the silver islands are much higher than the thickness of the SAM (∼2 nm), and there is no evidence of deposition in the SAM-covered regions.

Figure 2 show a series of AFM images of silver features deposited at different potentials onto gold surfaces patterned with ODT. At −0.45 V (Ag/AgCl), silver is deposited in the 6 μm surfactant-free squares, as described above, analogous to a positive resist in conventional lithography. At −0.55 V (Ag/AgCl), small silver islands are formed under the SAM-covered regions, although deposition still occurs predominantly in the SAM-free regions. At −0.65 V (Ag/AgCl), silver is deposited preferentially *under* the SAM-covered regions, analogous to a negative resist in conventional lithography. In contrast to the square islands formed in positive resist mode, deep square wells are formed in negative resist mode. While silver is deposited everywhere on the surface, the deposition rate in the SAM-modified regions can be more than twice that in the surfactant-free regions. This mode persists even for long deposition times, allowing significant differential feature heights to be realized between the SAM-modified and SAM-free regions. Finally, at −1.2 V (Ag/AgCl), deposition occurs uniformly over the entire surface, regardless of the original surfactant distribution.

The mode of deposition is dependent on potential and on the length of the alkane chain. Figure 3 shows a phase diagram summarizing the modes for silver deposition on patterned mono-

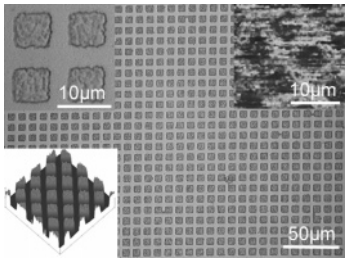

Figure 1. Plan view optical microscope image of 6 μm square silver islands deposited onto silver with an array of 6 μm surfactant-free squares at −0.45 V (Ag/AgCl) from 20 mM $KAg(CN)_2$. The deposition charge was 0.28 C cm^{-2}. The inset in the upper right is a friction force image of the ODT-patterned substrate prior to deposition showing the 6 μm square surfactant-free regions (dark). The inset in the upper left shows that the 800 nm high islands retain the fidelity of the pattern, illustrating that there is negligible lateral growth. The inset in the lower left corner is an AFM image of the 6 μm square silver islands.

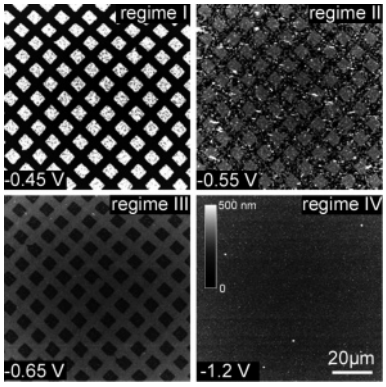

Figure 2. AFM images of silver features deposited onto an gold substrate with an array of 6 μm surfactant-free squares at −0.45, −0.55, −0.65, and −1.20 V (Ag/AgCl) from 20 mM $KAg(CN)_2$. In all cases, 0.15 C cm^{-2} silver was deposited.

[†] Department of Chemical and Biomolecular Engineering.
[‡] Department of Materials Science and Engineering.

10.1021/ja050955n CCC: $30.25

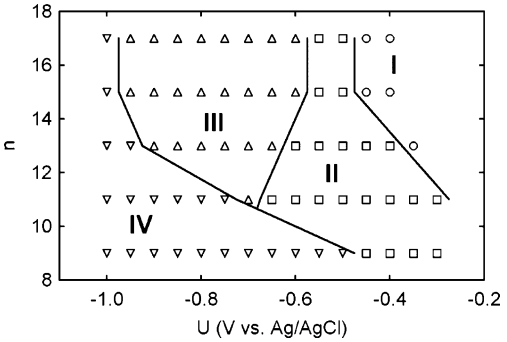

Figure 3. Phase diagram showing the four regimes for electrodeposition as a function of alkane chain length: (I) positive resist mode, (II) transition mode, (III) negative resist mode, and (IV) uniform deposition mode. In all cases, 0.15 C cm^{-2} silver was deposited from 20 mM $KAg(CN)_2$ onto patterned gold surfaces with 25 μm surfactant-free squares and 5 μm surfactant-free circles. The deposition mode was determined from AFM images.

layers of *n*-alkane thiols, with $n = 9$, 11, 13, 15, and 17. Four regimes can be identified.

At low overpotentials (regime I), the SAM-modified regions are positive resists for deposition, and the SAM acts as an insulating barrier or mask for deposition. Longer chain surfactants are more effective as positive resists, as evidenced by the negative shift in the onset potential for the transition mode (regime II) with increasing *n*. A surprising feature of this regime is that the lateral dimensions of the pattern are retained for feature heights much larger than the thickness of the SAM. For the features shown in Figure 1, lateral growth is negligible for feature heights below about 1 μm. Moffat and Yang[8] reported on the electrodeposition of nickel into stamped hexadecane thiol SAMs with 5 μm × 5 μm surfactant-free squares on copper and found that, up to a height of 120 nm, there was no lateral growth and the fidelity of the pattern was preserved. A possible explanation for this result is that the surfactant diffuses up the sides of the growing features, thereby suppressing lateral growth.

In the transition regime, deposition occurs under the SAM-modified regions as well as on the surfactant-free surface; however, the deposition rate is faster in the surfactant-free regions. Deposition in the SAM-modified regions is relatively uniform, indicating that the SAM becomes leaky to the metal ions. The extent of this regime increases with decreasing chain length, indicating that the SAMs become more permeable to ions.

We note that the potential limit of positive resist mode is close to the potential of zero charge, U_{zc}, reported for thiol-modified gold surfaces, which also becomes more negative with increasing chain length.[12] This result suggests that the reversal in sign of the electric field at the interface may play a role in the onset of breakdown of the SAM for electrodeposition. An implication of this observation is that, for $U > U_{zc}$, the electric field at the interface is parallel to the dipole moment associated with the thiol; however, for $U < U_{zc}$, the electric field is antiparallel to the dipole moment of the thiol. This effect may lead to permeability of the SAM. The potential limit of positive resist mode is also close to the potential at which alkanethiol SAMs exhibit a decrease in impedance, suggesting that they become leaky.[13]

At larger overpotentials, deposition occurs in both surfactant-free and SAM-modified regions; however, the deposition rate is faster in the SAM-modified regions. This is the negative resist mode (regime III). The onset potential for this regime is −0.6 V (Ag/AgCl) for $n = 15$ and 17; however, for shorter chain lengths, the onset potential is more positive. These results suggest that the SAM accelerates silver deposition. While this behavior is unexpected,

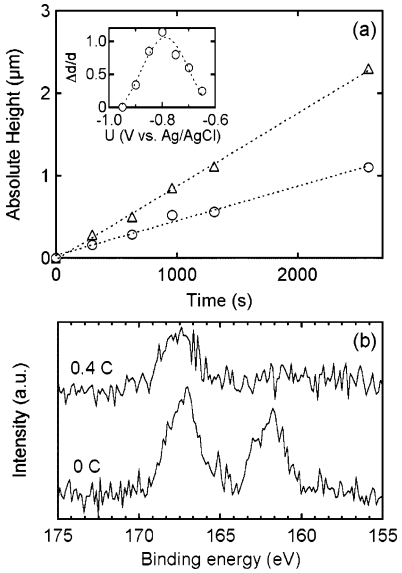

Figure 4. (a) Plot of the feature height versus time for the deposition of silver at −0.8 V (Ag/AgCl) (negative resist mode) onto ODT-patterned gold surfaces from 20 mM $KAg(CN)_2$. The inset is a plot of the normalized differential height versus potential for the deposition of 1 C cm^{-2} silver onto similarly patterned gold surfaces. (b) XPS spectra of the sulfur envelope before and after deposition of silver at −0.70 V (Ag/AgCl) onto ODT-patterned silver surfaces with 6 μm square surfactant-free regions for (i) 0 C cm^{-2} and (ii) 0.4 C cm^{-2}.

we note that the adsorption of SeCN accelerates the deposition of silver from $KAg(CN)_2$ on planar gold surfaces.[14] Similarly, the adsorption of short-chain dithiols accelerates the deposition of copper on planar gold surfaces from solution containing $CuSO_4$ and a suppressor, such as poly(ethylene glycol).[15]

The final regime in the phase diagram (regime IV) is at the most negative potentials, where deposition occurs uniformly everywhere on the surface, regardless of the original pattern. This is caused by loss of surfactant from the surface. For longer chain lengths ($n \geq 13$), the surfactant is reductively desorbed from the surface.[16] The onset potential for reductive desorption for a solution-formed ODT ($n = 17$) monolayer is −1.1 V (Ag/AgCl), slightly more negative than the onset of uniform deposition at −1.0 V (Ag/AgCl) (Figure 3). This shift is likely related to the poorer stability of stamped SAMs in comparison to that of solution-formed SAMs. For shorter chain lengths ($n \leq 13$), the onset potential for uniform deposition shifts to more positive potentials. The slope of this phase boundary is about 100 mV/*n*, much larger than the 20 mV/*n* shift seen in the reductive desorption peak for solution-formed SAMs.[16] This suggests that the solubility of the stamped thiol or an intermediate species formed during deposition shifts the onset potential for this mode positive to the reductive desorption potential.

Figure 4a shows the height of silver features in SAM-covered and SAM-free regions on an ODT-patterned gold surface in negative resist mode at −0.8 V (Ag/AgCl). The inset of Figure 4a shows a plot of the normalized differential height, $\Delta d/d$, of the features over the potential range spanning negative resist mode (see Figure 3). The normalized differential height increases with decreasing potential and reaches a maximum of 1.14 at −0.80 V (Ag/AgCl). At more negative potentials, as the boundary with regime IV is approached, $\Delta d/d$ decreases again. At the potential maximum, the growth rates, obtained from the slopes of the curves in Figure 4a, are 0.89 nm s^{-1} in the SAM-covered regions and 0.42 nm s^{-1} in the SAM-free regions.

Figure 4b shows an XPS spectrum of the sulfur envelope on a silver electrode patterned with ODT as a function of deposition

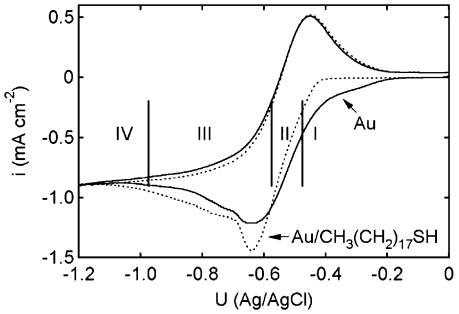

Figure 5. Cyclic voltammograms for Au and Au/ODT in 20 mM $KAg(CN)_2$ at a scan rate of 10 mV s^{-1}. The vertical lines indicate the boundaries of the deposition regimes shown in Figure 3.

time in negative resist mode. Prior to deposition, the spectrum shows two characteristic peaks: a thiolate peak at 162 eV and an oxidized thiol peak (e.g., $R-SO_3^-$, $R-SO_4^-$) at 167 eV.[17] The oxidized thiol peak remains after deposition of approximately 500 nm of silver under the SAM, confirming that the ODT remains on the surface in negative resist mode. These results indicate that the thiol floats on the surface during deposition.

Figure 5 shows cyclic voltammograms for gold and ODT-stamped gold in 20 mM $KAg(CN)_2$. Deposition on the ODT-modified surface is suppressed until about −0.45 V (Ag/AgCl), corresponding to the limit of positive resist mode seen in Figure 3. At about −0.6 V (Ag/AgCl), corresponding to the onset of negative resist mode, deposition on the ODT-modified surface becomes faster than on the bare gold surface. The deposition rate on the thiol-modified surface remains faster than on the bare gold surface over the potential range from −0.6 to −0.95 V, corresponding to the extent of negative resist mode in Figure 3. The difference in deposition rates does not reach the maximum value inferred from Figure 4, and hence, the influence of the patterned surface remains to be resolved. As described above, the limit of negative resist mode is close to the onset of reductive desorption of ODT, resulting in uniform deposition on the surface. Reductive desorption of the ODT results in almost identical curves in the reverse scans of the voltammograms.

The features of surfactant-based resists described above can be used to create complex, three-dimensional structures using sequential stamping in conjunction with deposition in positive and negative resist mode. We have also demonstrated that this approach can be extended to electroless deposition.

In summary, the behavior of patterned SAMs as templates for patterned electrodeposition is surprisingly rich. The deposition potential and chain length of the surfactant play an important role in determining the morphology of the deposited features. While many of the details of electrodeposition into patterned SAMs remain to be resolved, these results show that alkanethiol SAMs on gold or silver surfaces are tunable resists for the creation of complex structures by electrodeposition. The technique is simple and broadly applicable, requiring fewer steps than standard lithographic techniques for creating multicomponent, 3-D structures.

Acknowledgment. This work was supported by the JHU MRSEC (NSF Grant No. DMR00-80031). N.S.P. gratefully acknowledges support through a NASA graduate fellowship.

Supporting Information Available: Details of stamping and deposition. AFM images of thiol-patterned ($n = 17$, 13, and 11) gold surfaces after deposition of silver from 20 mM $KAg(CN)_2$. This material is available free of charge via the Internet at http://pubs.acs.org.

References

(1) Gau, H.; Herminghaus, S.; Lenz, P.; Lipowsky, R. *Science* **1999**, *283*, 46−49.
(2) Zhao, B.; Moore, J. S.; Beebe, D. J. *Science* **2001**, *291*, 1023−1026.
(3) Chen, C. S.; Mrksich, M.; Huang, S.; Whitesides, G. M.; Ingber, D. E. *Science* **1997**, *276*, 1425−1428.
(4) Tien, J.; Nelson, C. M.; Chen, C. S. *Proc. Natl. Acad. Sci. U.S.A.* **2002**, *99*, 1758−1762.
(5) Tiberio, R. C.; Craighead, H. G.; Lercel, M.; Lau, T.; Sheen, C. W.; Allara, D. L. *Appl. Phys. Lett.* **1993**, *62*, 476−478.
(6) Love, J. C.; Wolfe, D. B.; Chabinyc, M. L.; Paul, K. E.; Whitesides, G. M. *J. Am. Chem. Soc.* **2002**, *124*, 1576−1577.
(7) Xia, Y.; Whitesides, G. M. *Annu. Rev. Mater. Sci.* **1998**, *28*, 153−184.
(8) Moffat, T. P.; Yang, H. *J. Electrochem. Soc.* **1995**, *142*, L220−L222.
(9) Sonday-Huethorst, J. A. M.; van Helleputte, H. R. J.; Fokkink, L. G. J. *Appl. Phys. Lett.* **1994**, *64*, 285−287.
(10) Felgenhauer, T.; Yan, C.; Geyer, W.; Rong, H. T.; Golzhauser, A.; Buck, M. *Appl. Phys. Lett.* **2001**, *79*, 3323−3325.
(11) Kaltenpoth, G.; Volkel, B.; Nottbohm, C. T.; Golzhauser, A.; Buck, M. *J. Vac. Sci. Technol. B* **2002**, *20*, 2734−2738.
(12) Iwami, Y.; Hobara, D.; Yamamoto, M.; Kakiuchi, T. *J. Electroanal. Chem.* **2004**, *564*, 77−83.
(13) Boubour, E.; Lennox, R. B. *J. Phys. Chem. B* **2000**, *104*, 9004−9010.
(14) Baker, R. C.; Freeman, M.; Melnick, B.; Wheeler, D.; Josell, D.; Moffat, T. P. *J. Electrochem. Soc.* **2003**, *150*, C61−C66.
(15) Moffat, T. P.; Wheeler, D.; Josell, D. *J. Electrochem. Soc.* **2004**, *151*, C262−C271.
(16) Widrig, C. A.; Chung, C.; Porter, M. D. *J. Electroanal. Chem.* **1991**, *310*, 335−359.
(17) Hutt, D. A.; Cooper, E.; Leggett, G. J. *J. Phys. Chem. B* **1998**, *102*, 174−184.

JA050955N